LAWRENCE
LIVERMORE
NATIONAL
LABORATORY

UCRL-TR-218737

Feasibility of Single Molecule DNA Sequencing using Surface-Enhanced Raman Scattering

C. E. Talley, F. Reboredo, J. Chan, S. M. Lane

February 7, 2006

This work was performed under the auspices of the U.S. Department of Energy by University of California, Lawrence Livermore National Laboratory under Contract W-7405-Eng-48.

Feasibility of Single Molecule DNA Sequencing using Surface-Enhanced Raman Scattering
LDRD Project Tracking Code: 05-ERD-080
PI: Chad Talley
Co-Investigators: Fernando Reboredo, James Chan, and Steve Lane

Abstract

We have used a combined theoretical and experimental approach in order to asses the feasibility of using surface-enhanced Raman scattering (SERS) for DNA sequencing at the single molecule level. We have developed a numerical tool capable of calculating the E-field and resulting SERS enhancement factors for metallic structures of arbitrary size and shape. Measurements of the additional SERS enhancement by combining SERS with coherent anti-stokes Raman scattering (CARS) show that only modest increases in the signal are achievable due to thermal damage at higher laser powers. Finally, measurements of the SERS enhancement from nanoparticles coated with an insulating layer show that the SERS enhancement is decreased by as much as two orders of magnitude when the molecule is not in contact with the metal surface.

Background and Significance

It is widely recognized that single molecule sequencing (SMS) of DNA would be a revolutionary development in biology, biotechnology, medicine, and biosecurity. SMS promises to be simpler, cheaper, and quicker than present electrophoretic techniques that require multistep processing (preparation, cloning or amplification, fragmentation, electrophoretic separation, and interpretation).[1, 2] For many applications, SMS could become competitive with, and possibly more sensitive than microarray technologies for identifying sequences, and could be applied to samples where amplification is difficult or impossible.

For these reasons, several research groups have attempted to sequence DNA at the single molecule level over the past decade. While several approaches have been explored, including molecular force measurements[3] and nucleotide dependent electrical current measurements,[4] the majority of efforts have focused on optical methods based on single molecule fluorescence. One approach that has been explored is the use of exonuclease enzymes that cleave nucleotides, one at a time, from individual single-stranded DNA (ssDNA). Single nucleotides are then

detected downstream using exogenous fluorescent labels[5] or their natural fluorescence[6]. Similar approaches utilize DNA polymerase and monitor the incorporation of fluorescently labeled nucleotides.[7, 8] Many of these efforts are continuing, but to date, none of these approaches has yet been successful despite substantial government and commercial investment. The problems that plague these single molecule fluorescence based techniques are mostly due to their reliance on enzymes and exogenous fluorescent reporter molecules that have to be attached to the DNA bases.

In order to circumvent these problems, we propose to develop a single molecule sequencing scheme based on the intrinsic vibrational signature of the DNA nucleotides. This optically based technique requires no special labeling and does not require the use of enzymes. Instead, this technique uses large electric field enhancements from metal nanostructures combined with surface-enhanced Raman scattering (SERS). Raman spectroscopy provides chemically specific vibrational spectra that allow molecules to be identified. However, the Raman scattering process is a low probability event with typical cross-sections on the order of 10^{-30} cm^2. Because of these extremely low cross-sections, conventional Raman spectroscopy has been limited to concentrated samples and requires long integration times to produce spectra with sufficient signal-to-noise. In the 1970's three groups independently reported an anomalously high Raman scattering signal from molecules adsorbed onto roughened silver electrodes and termed the effect surface-enhanced Raman scattering (SERS).[9-11] These authors observed an increase in the Raman scattering signal of 10^6 over what was expected given the surface area of the films. This enhancement was attributed to an electromagnetic enhancement resulting from localized E-fields near the surface of the metal electrode and a chemical enhancement resulting from charge transfer between the metal and the chemisorbed molecule.

More recently, two groups independently observed the Raman scattering from *single* molecules adsorbed to metal nanoparticles.[12, 13] This observation requires 15 orders of magnitude of enhancement in the Raman scattering and, as a result, sparked a new interest in understanding the enhancement factors involved in SERS. Recent calculations have shown that at the junction between two nanoparticles separated by 1-3 nm, the E-field enhancement can approach 10^{12}. [14] This difference between the calculated E-field enhancement and the experimentally observed enhancement has been tentatively explained through two additional enhancement mechanisms: the chemical or charge transfer effect mentioned above and a

resonance Raman enhancement (most single molecule Raman experiments have been done with resonantly excited laser dyes).[15] It is still unclear whether the single molecule SERS requires that the molecule be in contact with the metal nanostructures to allow charge transfer and the resulting chemical enhancement. Several studies have shown that SERS enhancement is possible without direct analyte to metal contact, but not at the single molecule level.[16-19]

Research Activities

The aim of this research is to determine the feasibility of a single molecule DNA sequencing approach using surface-enhanced Raman scattering by answering three key questions.

I) Can resonant structures be designed to create an E-field enhancement that is sufficiently large and confined to observe the Raman scatter from single nucleotides in ssDNA?

This question is addressed through numerical calculations of metal nanostructures. The nanostructure serves a number of purposes: 1) it is a resonant structure that produces a large electromagnetic field enhancement, 2) it must also serve to confine the high field within a region small enough to mainly obtain a signal from a single nucleotide, and 3) it must physically confine the DNA molecule so that it remains within the high field region. Because the field enhancement is classical and the Raman cross-section scaling with field strength is well understood, much progress in the design of the optimum resonant nanostructure can be made by computational modeling and design. The computational methods of choice for electric field determination are the Finite Difference Time Domain (FDTD) approach and classical Mie scattering. Initial results with a commercial FDTD software package (XFDTD, Remco, Inc.) suggested that an alternative method would need to be developed to calculate a range of structures with arbitrary shapes and sizes. We therefore developed a quasi-static finite element approach for calculating arbitrary structures. A range of geometries including various arrangements of nano- spheres, rods, cones, wedges, etc. have been investigated.

II) Can SCARS give additional super-enhancement of the SERS?

In order to increase the E-field at the metal surface, we have coupled SERS with another technique known as coherent anti-stokes Raman scattering (CARS). In CARS, two phase matched beams differing in frequency by the molecular vibration of interest, are focused onto the

sample. In this way the vibrational mode is resonantly pumped increasing the photon scattering rate from the selected vibrational mode. Calculations have shown that by combining the two techniques SERS and CARS to a new technique, dubbed SE-CARS (surface-enhanced coherent Anti-Stokes Raman scattering), Raman scattering enhancements of 10^{21} could be achieved![20] Our group at LLNL is one of very few research programs that is simultaneously performing research in both of these areas (SERS+CARS) and is thus well positioned to test these predictions. We have investigated the increase in the Raman scattering signal that is obtained by combining these two techniques for silver nanoparticles. The increased signals from SE-CARS may be critical for practical SMS.

III) Is contact between the analyte molecule and the metal surface required for single molecule SERS?

The literature is undecided on this point: several researchers claim that electric field effects are sufficient to describe the observations while others claim that a chemical effect (probably involving electron transfer from the nanostructure to the molecule) is necessary to explain the observations. One way we will address the issue of whether or not a chemical attachment is necessary to achieve single molecule detection with SERS is by preparing nanoparticles 60-80 nm in diameter and coating them with a thin (1-2 nm) layer of SiO_2. These particles will then be aggregated in the presence of Rhodamine 6G. For comparison we will also carry out these experiments with uncoated nanoparticles, which have been shown to have single molecule sensitivity. These experiments are designed to provide an estimate of the loss in Raman scattering signal as the molecule is separated from the metal surface.

Results /Technical Outcome

I) Numerical Simulations of SERS Structures

Surface plasmons on metallic nanostructures of different geometries were calculated within the quasi-static approximation which is valid in when the dimensions of the structure are much smaller than the wavelength of light. Within these conditions, one can ignore retardation effects and assume static Coulomb interactions. Nanostructures of different shapes were modeled as a classical electron gas with neutralizing positive background (Drude model). In the quasi static approximation the surface plasmon modes and the bulk excitations are decoupled. A surface

plasmon is a self-sustained oscillation of the electron gas which results in an oscillating surface charge density and an induced electric field. We have developed a finite element tool to obtain these self-sustained surface plasmons for arbitrary geometries. We have derived a figure of merit for SERS applications. Using this figure of merit we have evaluated different shapes for SERS. We have found structures that are 12 orders of magnitude more efficient than spheres that are in principle possible to fabricate with current techniques.

Model and method

If one applies a uniform electric field to an electron gas in a metallic nanostructure, the electric field will displace the negative charge of the electrons from the neutralizing positive background (see Figure 1). For small displacements, the surface charge can be approximated by a two dimensional charge density $\sigma(\mathbf{r})$.

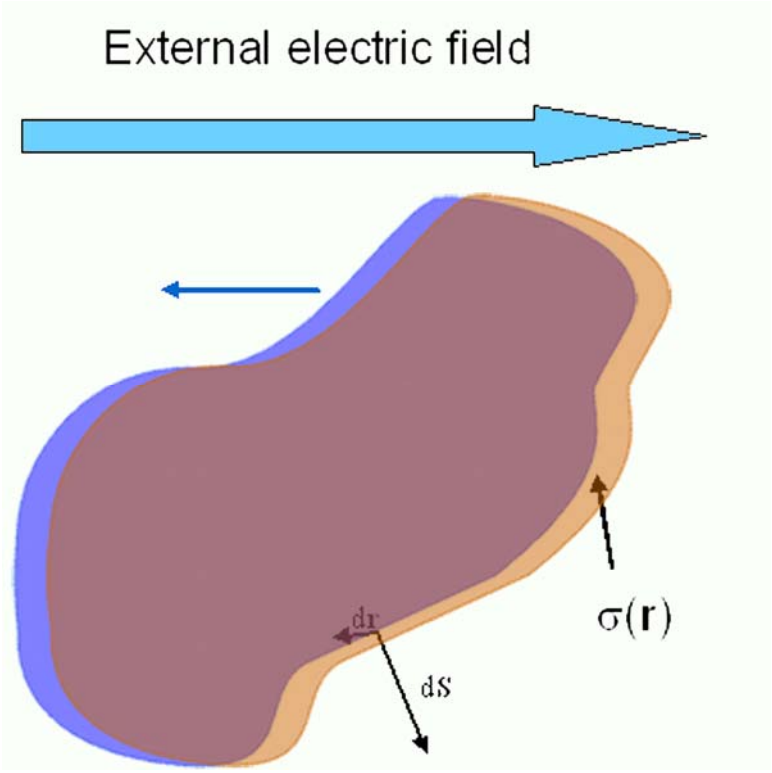

Figure 1: Surface charge generated on a metallic object by an instantaneous external electric field.

As soon as $\sigma(\mathbf{r})$ is different from zero, the field acting on the electron gas is no longer the external electric field but a superposition of the external electric field and the induced surface charge field. Plasmons are self-sustained oscillations of the electron gas, they are sustained by the induced charge field only. They can be excited with an external electric field under resonance conditions to generate high electric fields at the immediate vicinity of the surface.

When the dimensions of the particles are much smaller than the wavelength of light, one can ignore retardation effects. The instantaneous induced electric field in a given point $(\vec{r})$ is given by the Coulomb interaction. That is

$$\vec{E}_{ind}(\vec{r}) = \int_S dr'^2\, \sigma(\vec{r}')\frac{(\vec{r}-\vec{r}')}{|\vec{r}-\vec{r}'|^3}, \qquad (1)$$

Where $\int_S dr'^2$ denotes an integral restricted to the nanostructure surface. Within the linear response (small electric fields and displacements) and within the Drude model, the velocity of the electron gas electron gas inside the metal is proportional to integral of the acceleration, which in turn is proportional to the electric field. After performing a Fourier transform, for a given frequency ω, the velocity $\vec{v}(\vec{r},\omega)$ is

$$\vec{v}(\vec{r},\omega) = \frac{e^2}{i\omega\, m}\int_S dr'^2\, \sigma(\vec{r}')\frac{(\vec{r}-\vec{r}')}{|\vec{r}-\vec{r}'|^3} \quad , \qquad (2)$$

with e being the electron charge and m the electron mass. The current inside the nanostructure is

$$\vec{j}(\vec{r},\omega) = n_0\vec{v}(\vec{r},\omega). \qquad (3)$$

Since the $\nabla\vec{E}_{ind}(\vec{r}) = 0$, for every point not included in the surface, the divergence of the current is also zero inside the nanostructure. Accordingly, there is no bulk induced charge as a result of a surface induced field, which means that surface and bulk modes are decoupled within this approximation.

The surface charge $\sigma(\vec{r})$ (see Figure 1) is proportional to the component of displacement $d\vec{r}(\vec{r})$ perpendicular to the surface $d\vec{S}(\vec{r})$

$$\sigma(\vec{r}) = n_0 d\vec{r}(\vec{r}) \bullet d\vec{S}(\vec{r}). \qquad (4)$$

Since the displacement $d\vec{r}(\vec{r})$ is in turn the integral of the velocity then

$$\sigma(\vec{r}) = n_0 \frac{v(\vec{r})}{i\omega} \bullet d\vec{S}(\vec{r}) = -\frac{4\pi\omega_p{}^2}{\omega^2} \int_S dr'^2\, \sigma(\vec{r}\,') \frac{(\vec{r} - \vec{r}\,') \bullet d\vec{S}(\vec{r})}{|\vec{r} - \vec{r}\,'|^3} \qquad (5)$$

that can be rewritten as

$$4\pi \int_S dr'^2\, \sigma(\vec{r}\,') \frac{(\vec{r} - \vec{r}\,') \bullet d\vec{S}(\vec{r})}{|\vec{r} - \vec{r}\,'|^3} = \frac{\omega^2}{\omega_p{}^2} \sigma(\vec{r}) \qquad (6)$$

with ω_p being the bulk plasma frequency. In order to obtain both the resonant frequencies ω_n and their associated surface plasmon modes $\sigma_n(\vec{r})$, we have to search for the eigenvalues and eigenvectors of (6). We did so using the finite element method explained in the following section. Eq. (6) has always a solution with $\omega_0 = 0$ that corresponds to the equilibrium configuration of surface charge for a charged metal. One important detail of Eq. (6) is that the operator acting on $\sigma(\vec{r}\,')$ is size independent. That means that within this approximation the eigenvalues of Eq. (6) are only dependent on the shape of the structure but not on size.

In order to conclude this theoretical section let us now concentrate in the coupling with the external electric field. A uniform external electric field $\vec{E}$ applied during and infinitesimal time dt induces a charge density of the form

$$\sigma_E(\vec{r}\,') = n_0 \vec{E} \bullet d\vec{S}(\vec{r}) dt \qquad (7)$$

Being $\vec{E} \bullet d\vec{S}(\vec{r})$ a unit vector normal to the surface $\sigma_E(\vec{r}\,')$ has, in principle, components in every mode of the system and can be expressed as a linear superposition of surface plasmon components:

$$\sigma_E(\vec{r}\,') = \sum \sigma_n(\vec{r}\,') \int dr^2 \sigma_n(\vec{r}) \sigma_E(\vec{r}) dS = \sum \sigma_n(\vec{r}\,') \int dr^2 \sigma_n(\vec{r}) \vec{E} \bullet d\vec{S}(\vec{r}) \qquad (8)$$

with $\int dr^2 \sigma_n(\vec{r}) \sigma_m(\vec{r}) dS(\vec{r}) = \delta_{n,m}$ (9)

Thus the external electric field excites each a plasmon mode with amplitude

$$E_n = \int dr^2 \sigma_n(\vec{r}) \vec{E} \bullet d\vec{S}(\vec{r}). \qquad (10)$$

For a given frequency of ω, the external field excites each normal mode individually as a harmonic oscillator under an external applied field E_n. The response of the system is a superposition of the response of each normal mode. That is, the induced surface charge density is given by

$$\sigma_{ind}(\vec{r}',t) = e^{i\omega t}\sum \varepsilon(\omega,\omega_n)\sigma_n(\vec{r}')E_n \quad , \tag{11}$$

where $\varepsilon(\omega,\omega_n)$ has the same structure of the Drude dielectric function but replacing ω_p by ω_n.

Using the Gauss theorem, it is also easy to obtain the normal component of the electric field infinitesimally outside the nanostructure. For a given normal mode, the maximum normal induced electric field is given by the following expression

$$E_{ind}{}^{\max}(\vec{r}',t) = \varepsilon(\omega,\omega_n)\left(4\pi - \frac{\omega_n{}^2}{\omega_p{}^2}\right)\sigma_n(\max)\int dr^2\sigma_n(\vec{r})\vec{E}\bullet d\vec{S}(\vec{r}) \tag{12}$$

Note that all the materials properties are included in $\varepsilon(\omega,\omega_n)$, the remaining factors in Eq. (12) are only dependent on shape (they are size independent). We define a figure of merit with as

$$Fm = \left(4\pi - \frac{\omega_1{}^2}{\omega_p{}^2}\right)\sigma_1(\max)\int dr^2\sigma_1(\vec{r})\vec{E}\bullet d\vec{S}(\vec{r}) \tag{13}$$

The equation to optimize for obtaining maximum response for SERS is Eq. (13). Eq. (13) can be evaluated analytically for a sphere $Fm(sphere) = 8\pi/3$. We will use the spherical shape as a reference. Different materials will rescale the frequencies of the plasmons; thus the ratios $\frac{\omega_n{}^2}{\omega_p{}^2}$ are independent of size and material. Thus two structures with the same shape will have the same the same figure of merit in Eq. (13). The smaller (larger) structure will have a larger (smaller) $\sigma_n(\max)$ that will be exactly compensated by a smaller (larger) coupling with the external field E_n (see below). However, a shape that is a combination of two structures with the same frequency can combine a large $\sigma_n(\max)$ and large E_n. Self similar structures fall in this category and have been proposed as possible surface plasmon amplifiers. Let us consider a particular shape of size L with a first exited mode $\sigma_1(\vec{r})$ with figure of merit Fm. The normalization condition in Eq. (9) determines that $\sigma_n(\vec{r})$ scales with size as $\sim 1/L$. In turn E_n scales as $\sim L$. Thus, since the frequency of the surface plasmons is independent of size, the

plasmons of a structure of size L will hybridize with the ones of a structure with size αL giving rise to a plasmon mode with amplitude

$$\tilde{\sigma}(\vec{r}) \approx \frac{\left(\sigma_1(\vec{r}) + \sigma_1(\alpha\ \vec{r})/\alpha\right)}{\sqrt{2}} \quad , \tag{14}$$

and coupling constant

$$\tilde{E} \approx \frac{\left(E_1 + E_1\alpha\right)}{\sqrt{2}} \quad . \tag{15}$$

Therefore, for $\alpha >> 1$, the combination has a figure of merit

$$\tilde{F}m \approx Fm(1+\alpha)/2, \tag{16}$$

similarly structure a combination of N self similar structures will have a figure of merit $\tilde{F}m \approx Fm(1+\alpha_2 + \cdots + \alpha_N)/N$. Since there is a denominator N, there is little gain by combining more than two. We emphasize here that this amplifying effect will only hold as long as the hybridization model remains valid.[21, 22] That implies that the coupling cross elements are smaller than the eigenvalue differences in Eq (6). Since the couplings come from the Coulomb interaction of different modes, the requirement of small couplings sets limits on the proximity of the structures. This amplification only occurs if the localized and extended surface plasmons are entangled by a Coulomb coupling. This implies that the differences on the frequency squares of the two plasmons must be smaller than the coupling term. This in turn set limits on the tolerances and errors that are imposed to the experimental realization of these structures. We will show that a proper description of the curvature is very important for the determination of the surface plasmons. Which implies that a proper control of the curvature is also very important to achieve large amplifying effects.

Numerical solution of the eigenvalue problem

We solved Eq. (6) with a simple finite difference method, that consist in breaking up the nanostructure surface into a set of flat or curved triangles. The surface charge is assumed to be constant within each finite element. Thus the integral eigenvalue in Eq. (6) is replaced by matrix eigenvalue equation

$$\sum_j K^{i,j}\sigma^j(\vec{r}) = \lambda\sigma^i(\vec{r}) \tag{17}$$

For $i \neq j$, the matrix elements of $K^{i,j}$ is the normal component electric field at center of mass of element i created by a uniform charge at element j which is integrated numerically. The $i = j$ case is the electric field inside the surface created by the curved finite element i. This electric field can be approximated as

(18)

$$Kii = 2\pi + \oint \frac{\mathbf{dl}.\boldsymbol{\rho}^{\perp}(l)}{\rho(l)^2}\alpha(l)$$

Where the integral is done over the contour l of the finite element "i", and the finite element is expanded in the plane normal to the center with coordinate $\boldsymbol{\rho}$ and a direction dependent curvature $\alpha(l)$. Eq (12) is integrated numerically. [1]

In Fig. 1 we compare the numerical results obtained with our numerical approach with the exact solutions obtained analytically for a spherical shell which are given by

$$\omega^2(\pm) = 2\pi \frac{e^2 n_0}{m}\left\{1 \pm \frac{\sqrt{1+4(b/a)^{2l+1}l(l+1)}}{2l+1}\right\} \quad . \qquad (19)$$

[1] The numerical method is currently implemented in a Mathematica package that is available to anyone upon request to the corresponding author.

Where a and b are the exterior and interior radii of the shell respectively, and l the angular momentum of the plasma excitation. . The continuous lines in Figure 1 mark the solutions of Eq. (19) for different values of the angular momentum l. The dots denote the numerical solutions of the eigenvalue problem solved numerically. The calculations were done for $b/a = 1/2$ using 960 finite elements for the complete system.

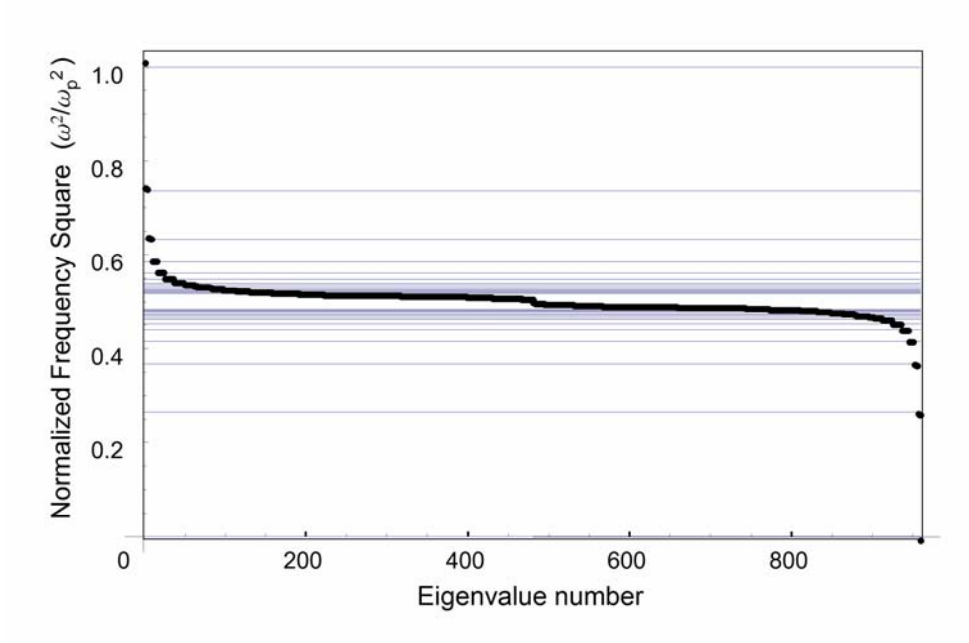

Figure 2: Analytical solutions for a spherical shell with b/a = ½ for different angular momenta (continuous lines). Numerical results obtained with a finite element approach (dots).

We find an excellent agreement between exact theory and numerical results. This agreement was corroborated for additional geometries such as a sphere adjacent to an infinite plain a pair of spheres etc.

Once we have established the accuracy of our theoretical approach with well known theoretical results we can embark ourselves in the study of other geometries which cannot be solved analytically. In Figure 3 we show the surface plasmons associated with a hole on a film. The red and blue colors denote charge of opposite sign while gray denotes zero. The shape of the hole was chosen for numerical convenience (not optimized) to be a revolution surface of the form

$$x = g(t); y = \cos(\phi)f(t); z = \sin(\phi)f(t) \qquad (20)$$

with

$g(t) = \tanh(t); \quad f(t) = 1/\left[1 - g(t)^2\right].$

These equations define a hole of diameter 2 on a film of width 2.[i] The mesh is equally spaced in the parametric variables "t" and ϕ, thus there is more resolution at the hole location. We see in figure 3, that the surface density decays as a function of the radius therefore a description of the film outside a given cutoff is unnecessary. The surface plasmon frequency is 0.45 ω_p . The figure of merit of this hole, which was not optimized at any rate is factor 16.8 beter than a sphere which means that a film hole like this could be at least $8x10^4$ better for SERS than a perfect sphere.

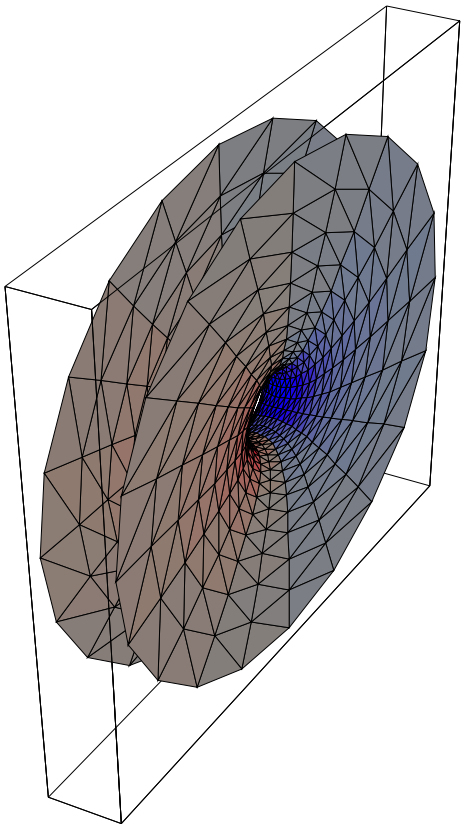

Figure 3: Surface plasmon localized at a hole in a metallic film. The lines mark the finite element mesh. The red and blue color correspond to surface charge density of opposite sign, gray marks neutral regions.

We mentioned in the theory section, that amplification can be achieved by combining together two or more structures with matching frequencies. We will explore a couple of examples in the rest of this paper. The first example will be this hole on a spherical shell and second a landscaped hole on a film.

Hole on a spherical shell

Equation (19) shows that the frequencies of the surface plasmons of an spherical shell can be tuned by changing the internal to external ratio b/a . We thus can adjust the shell so as it matches the frequency of a hole and build a combined system. Figure 4 shows the calculated first excited surface plasmon for a shell with $a = 5.61$ and $a = 3.61$ and a hole of diameter 2 similar to the one of Fig. 3.

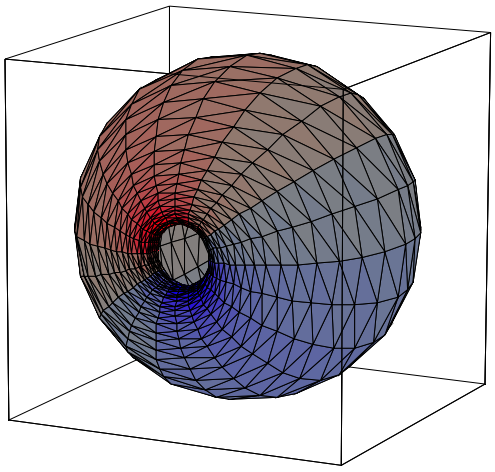

Figure 4: Surface plasmon localized at a hole in a metallic shell. Same conventions as in Figure 3.

As expected by design, the lower energy excitations should be a symmetric combination of a hole plasmon mode with a shell plasmon mode. Figure 4 shows that the surface plasmon extends well beyond the hole and to the spherical resonant shell. Because the system has cylindrical symmetry the excitation is degenerate (there is another excitation rotated 90 degrees with the same frequency). Since the hole and the shell mode are coupled, the frequency of these modes is slightly smaller ($0.40\ \omega_p$) than the isolated hole or shell. Although we expected a larger figure of merit in the combination, we find surprisingly the same figure of merit than the isolated hole (*fm* is 16.8 larger than the spherical shape). Nevertheless, this figure of merit is much larger than the perfect shell (without the hole Fm = 6.5). Thus a shell with holes can be at least 44 times more efficient than a perfect shell for SERS. Accordingly, holes should be promoted rather than avoided in shell synthesis for SERS.

We can understand the value obtained for Fm for this combination as follows. Although the structure in Fig 4 is not self similar, we can use Eq. (16) to understand why we do not get a significantly larger Fm. The are to main reasons i) the shell is not much larger than the hole, only

a factor $\alpha \sim 5$. Since there is a denominator 2 in Eq. (16) little is gained with the combination. ii) In addition, the normal to the surface has opposite directions at the hole and at the external surface of the shell. Thus there are contributions of opposite sign to the coupling with the External field in Eq (10). Which means that, instead of adding one to the other, like in Eq. (15), the contributions from the hole and the surface cancel each other in Eq.(10). Thus the coupling to the external electric field of the combination is smaller than depicted in Eq. (15). The fact that we find numerically the same figure of merit is just by chance.

Landscaped hole

While we have shown that is possible to design a system that couples a localized and an extended surface plasmon modes. It remains to be shown than we can use this effect to obtain large amplifications in the figure of merit. In this section we will show that it is in fact possible to landscape a hole so as the figure of merit can be drastically increased. The shape of the structure that we characterized is generated by circular revolution of a two dimensional shape. In Figure 5a we provide the two dimensional shape that generates the landscaped hole shown in Figure 5b and 5c.

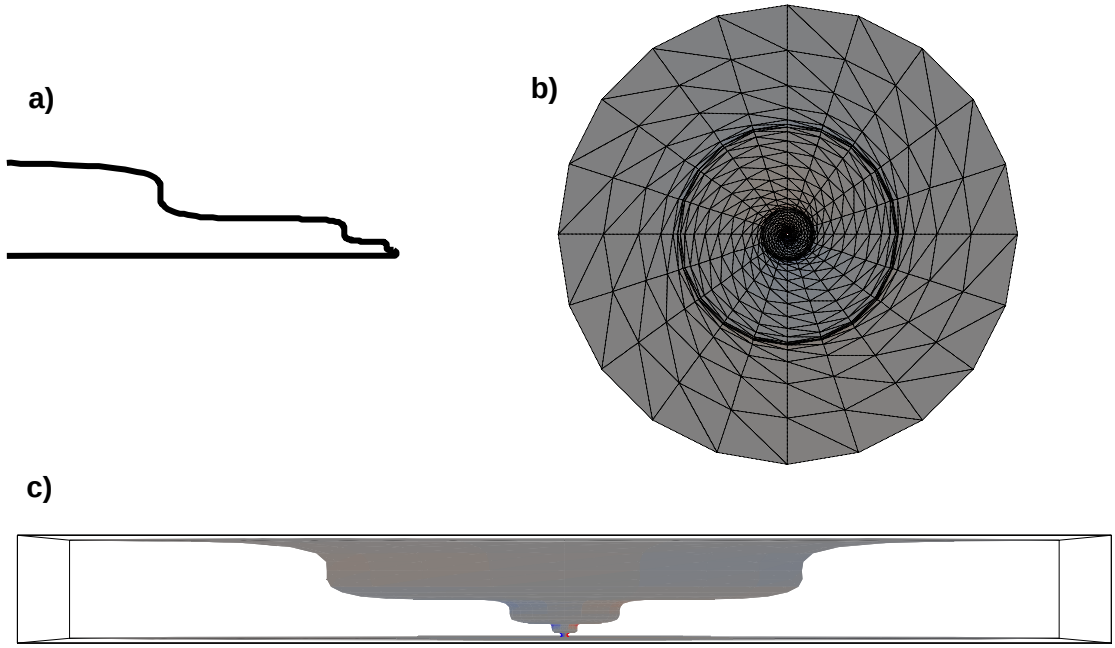

Figure 5: Landscaped hole on a metallic film with three bumps a) Revolution shape of the hole b) Top view of the hole c) Side view of the hole cross section.

The hole was designed for theoretical convenience and was not optimized. Nevertheless, it has some self similarities. We have also designed the hole to be asymmetric so it could be potentially fabricated with focus ion bean (FIB) on a metallic film or other etching techniques. The upper surface of the film within the interval of radius from the hole of $\rho = 3^4 = 81$ and $\rho = 3^0 = 1$ is given by the following equations

$$
\begin{aligned}
&z = h(x) = \mathrm{Log}(\lambda)\left[1/\mathrm{Log}(\lambda) - Sin(2\pi x)/(2\pi)\right]\lambda^x \\
&\rho(x) = \mathrm{Log}(\nu)\left[1/\mathrm{Log}(\nu) + Sin(2\pi x)/(2\pi)\right]\nu^x \\
&\mathrm{y} = \rho(x)\sin(\varphi)\ ;\mathrm{x} = \rho(x)\cos(\varphi) \qquad (21)\\
&\text{with } \lambda = Exp\left(4/n_b Log(2)\right) \\
&\text{and } \nu = Exp\left(4/n_b Log(3)\right)
\end{aligned}
$$

Thus when one runs x from 0 to n_b, ρ will grow from 1 to 81 and z will grow from 1 to 16 with the number of bumps in the resulting shape will be n_b. For n_b = 4, for example, ρ will grow a factor 3 before a bump and z will multiply by 2 after a bump. Thus each bump will "see" a similar local shape inside: an interior bump of one third of it radius where the width of the film is reduced one half. The innermost hole is closed by a torus surface of internal radius 1 and cross section diameter 1. The lower surface of the film is just a plane with a circular hole at the center. Different values of n_b will give different landscapes for around a central hole in the same film. In Table 1 we give the maximum figure of merit of all the modes in the system in units of the spherical shape Fm as a function of the number of bumps n_b.

n_b	1	2	3	4
Figure of merit	1329	974	831	790

Table 1 Figure of merit as a function of the number of bumps for the shapes of Fig 5.

As can be seen in Table 1, the results are striking. They are more striking if one takes into account that the shape of the bump is not even optimized. It was chosen for numerical convenience. Moreover, the bumps are not strictly self similar (only if one ignores the smaller curvature along the angle ϕ). Instead we preferred to increase the scale along ρ (which lowers the resonance frequency but improves α). The figure of merit is larger for a single bump than form

many. The values found are three orders of magnitude beter than perfect spheres and to more than single holes. These structures are 12 orders of magnitude better than perfect spheres for SERS. The structures found offer a promising avenue to amplify surface plasmons at holes in thin films. A molecule like DNA could be potential thread in the hole and read base by base with a Raman signal.

II) Surface-enhanced Coherent anti-Stokes Raman Scattering (SE-CARS) Spectroscopy

Experiments were performed to measure the enhancement acheiveable by implementing a combination of surface-enhancement using metal nanoparticles and CARS spectroscopy to tune into a particular molecular vibration of interest. Figure 6 illustrates the setup, which consists of two Ti:Sapphire lasers tunable from 750 – 950 nm running at 80 MHz repetition rate. The lasers are electronically locked so that the pulses can be overlapped in time. The two beams are collinearly combined into an inverted microscope and focused into the sample using a high NA

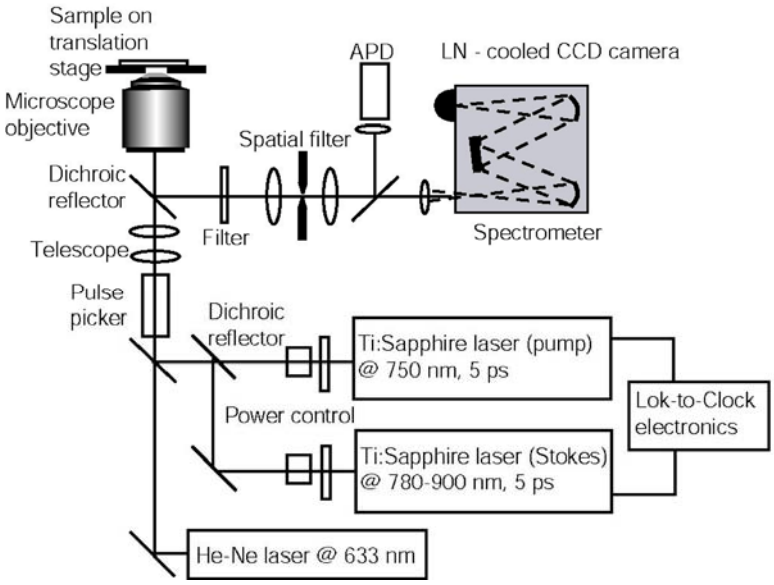

Figure 6 Schematic of CARS and Raman confocal microscope

oil immersion objective. CARS signals are epi-detected and delivered through a confocal pinhole and can be sent either into a spectrometer or a single photon counting avalanche photodiode (APD). In addition, the two beams can be introduced into a pulse picker, which is used to reduce the repetition rate of the laser beams down to as low as 80 kHz while maintaining high peak energy. The setup also consists of a 633 nm He-Ne laser that is also collinear with the CARS

laser beams. This laser can be used for surface enhanced Raman spectroscopy (SERS) on the same samples.

Two different samples were used in this study. Silver nanoparticles coated with either 4-mercaptobenzoic acid (4-MBA) or rhodamine 6G (R6G) were used to test the SE-CARS method. The samples were prepared by mixing approximately 3 microliters of 4-MBA or R6G in 0.5 mL of silver nanoparticle solution. These samples have previously been shown to yield SERS spectra with sharp Raman vibrations[23]. The wavelength of the Ti:Sapphire beams were tuned into either the 1590 cm^{-1} vibration of 4-MBA or the 1358 cm^{-1} vibration of R6G. These vibrations were chosen due to their large Raman cross-section. For 4-MBA, the Ti:Sapphire laser wavelengths were 750 nm and 851 nm. For R6G, the wavelengths were 750 nm and 835 nm. The nanoparticle samples were prepared two different ways for SE-CARS analysis. First, coated nanoparticles were dried out onto a glass coverslip. Detection of the nanoparticles was achieved by scanning the 633 nm laser beam (~1 mW) over the sample to generate a SERS image point by point using the APD. The two Ti:Sapphire beams were then positioned onto each individual nanoparticle and a CARS signal was acquired using the spectrometer. A second alternative method involved adding a 50 microliter solution of the coated nanoparticles onto a glass coverslip and focusing the laser beams directly into solution.

Figure 7a shows a SERS image of nanoparticles dried onto a coverslip. Figure 7b shows the SERS spectra of 4-MBA. These nanoparticles were damaged when exposed to the two Ti:Sapphire beams running at full 80 MHz repetition rate and average powers of 20 and 10 mW. The damage was confirmed by exposing the nanoparticle to the Ti:Sapphire beam for 1 second, and then attempting to acquire a SERS spectra from that particle. As shown in Figure 7c,

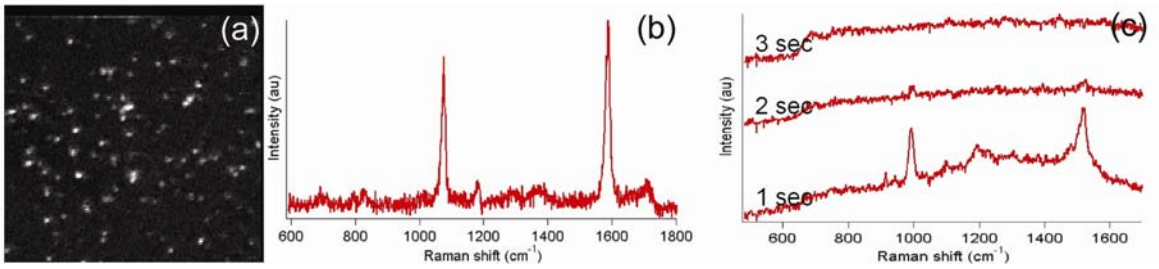

Figure 7 (a) SERS image of 4-MBA coated silver nanoparticles dried on a glass coverslip. (b) SERS spectrum of 4-MBA, taken by focusing a 633 nm laser beam onto a bright region in (a). (c) Exposure

repeated exposure to the Ti:Sapphire beams reduced the SERS signal intensity significantly. Following this observation, we measured the range of powers and repetition rates that we could use for the Ti:Sapphire beams which would not damage the nanoparticles.

Table 2 illustrates the repetition rate, average power, and corresponding peak energy that were tested that resulted in no particle damage. Of particular interest were the 80-100 kHz repetition rates, which allowed us to use 150 – 240 microwatts of average power without particle damage. At these conditions, a peak energy as high as 3×10^{-9} J was attainable. Since CARS is an intensity dependent process (CARS signals is proportional to the intensity of the Stokes laser beam and square of the intensity of the pump laser), achieving these high energies should allow us to generate a CARS signal. However, repeated efforts to generate a SE-CARS signal under these conditions were unsuccessful due to a large background fro immobilized nanoparticles. This large background arises from a CARS signal can readily be generated at an oil-coverslip interface, due to discontinuities in the χ^3 at interfaces[24]. This undesired CARS signal was a major problem when attempting to detect and discriminate the CARS signal from molecules attached to nanoparticles adhered so closely to the coverslip surface.

Rep rate	Average P (uW) (no damage)	Peak Energy (J)
80 MHz	420	5.25e-12
800 kHz	400	5.00e-10
80 kHz	240	3.00e-9
150 kHz	180	1.2e-9
100 kHz	150	1.5e-9
400 kHz	240	6e-10

Table 2. Laser parameter conditions that resulted in no noticeable damage to the nanoparticles.

An alternative scheme involved probing nanoparticles that are suspended in solution. This scheme is similar to that described by Koo et. al[25], who applied SE-CARS for single molecule detection. In this configuration, the laser beams are focused through the coverslip and into a 50 microliter solution of coated nanoparticles. Since the laser focal volume is on the order of 1 μm^3, particles floating in and out of this volume will generate a burst of CARS/SERS signal. In addition, it was observed that the laser beams influence the directional motion of the nanoparticles, drawing them into the laser focus as a result of optical trapping effects. However, the metallic nanoparticles cannot be stably trapped due to the large scattering forces, so there is a constant exchange of nanoparticles in and out of the focal volume. Figure 8 shows the SE-CARS signal (blue) from 4-MBA coated nanoparticles. The acquisition time for this spectrum was 500 milliseconds and maximum powers from the lasers were used, roughly 200 mW total at the microscope. The signal is at 670 nm, as expected. Also shown in the figure is the signal from nanoparticles without 4-MBA (black). A signal can be observed from bare nanoparticles due to the nonresonant background inherent in CARS spectroscopy, as well as the fact that bare nanoparticles perpendicular to the optical axis creates an interface, and the χ^3 discontinuity[24] between two media generates an epi-CARS signal. We attribute our ability to acquire a signal from these particles in solution without damaging due to the fact that the particles are constantly in motion in and out of the focus.

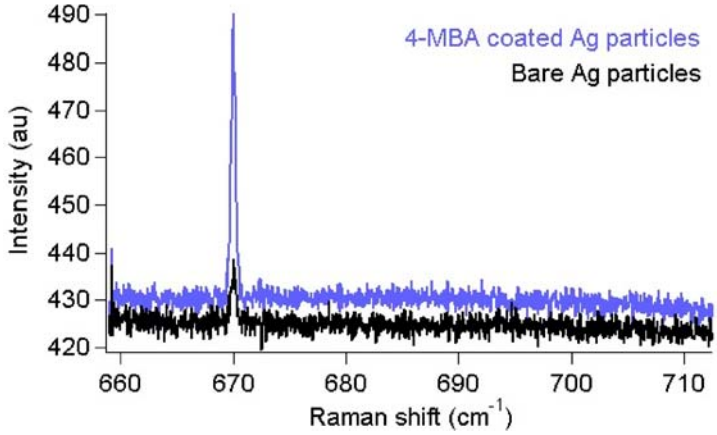

Figure 8 SE-CARS signal (blue) from 4-MBA coated silver particles from the 1590 cm-1 Raman vibration. Shown in black is the signal from bare silver particles.

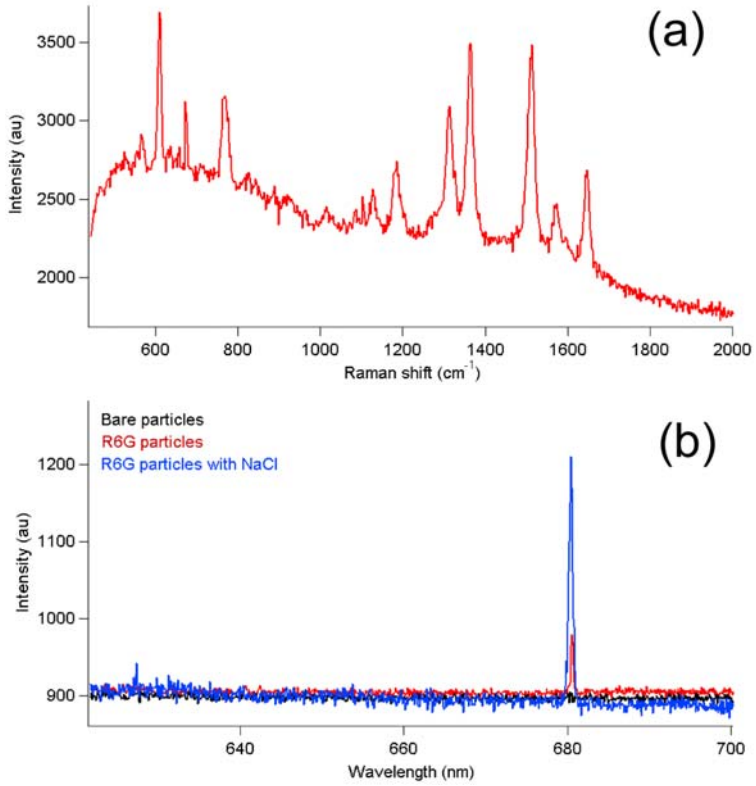

Figure 9 (a) SERS spectrum of R6G on silver nanoparticles in solution, taken with 8 mW 633 nm laser beam and a 30 second integration time (b) SE-CARS signal (red) located at 680 nm, due to coherent vibration of the 1358 cm^{-1} R6G Raman peak. The addition of NaCl appears to increase the signal dramatically due to nanoparticle clustering. Also shown, in black, is the signal from bare particles in solution.

In order to quantify the enhancement effect of SE-CARS over SERS, we probed the SERS and SECARS spectra of R6G-coated silver nanoparticles. R6G was chosen for this analysis because it has a stronger SERS signal than that of 4-MBA. The final concentration of R6G in this sample was approximately 100 nM. Figure 9 shows the SERS spectrum of R6G, acquired for 30 seconds using 8 mW of 633 nm laser power, giving a signal of 1100 counts for the 1358 cm^{-1} peak. We are able to detect this signal at 30 counts with a 1 second integration time (not shown). With SE-CARS, using 200 mW total power, we detect a SE-CARS signal of 100 counts with only a 100 ms integration time (see Figure 9b). The enhancement is only on the order of a factor of 2, taking into account the different average powers used and the different integration time. We would expect a stronger enhancement, as has been reported previously by Koo et. al.[25], but have not determined the reason for this discrepancy. It should be pointed out

that the addition of NaCl to the nanoparticle solution increased the SE-CARS signal (figure 9b), which can be attributed to the clustering of silver colloids leading to the enhancement of signals at nanoparticle junctions.There are still many issues that remain to be addressed. The most important deals with the low contrast in CARS signal intensity from coated and uncoated particles. In general, particles coated with either 4-MBA or R6G were able to generate a strong SE-CARS signal. However, it was observed that bare particles also generated very intense signals at equivalent wavelengths. At times, it was observed that the magnitude of these signals was of the order of the signals from coated nanoparticles. It is unclear why the resonant enhancement from the molecules is inconsistent and not as strong as expected. Applying variations to CARS, such as the use of polarization CARS, may help to suppress the undesired nonresonant background and isolate the signal coming solely from the molecules. Another issue to investigate further is the issue of signal strength. These particles are fully saturated with molecules, and only give off a relatively weak SE-CARS signal. To achieve single molecule detection, improvements need to be made to the experimental method, either by developing more consistent junctions between particles or reevaluating the use of pulse picked beams to achieve high peak energy without the possibility of damage.

III) Estimating the loss of enhancement without molecule-metal contact

One factor that would reduce the read length possible with the proposed SERS sequencing scheme is the requirement of contact between the metal and the molecule in order to achieve enough enhancement for single molecule detection. In order to estimate the amount of enhancement lost by lack of contact with the metal surface, we have performed experiements in which the enhanced molecule is separated from the metal surface by a dielectric.

Silver nanoparticles were prepared by the reduction of silver nitrate with sodium citrate as described in the literature. The silver nanoparticles were then coated with mercaptopropylsilane and sodium silicate was allowed to polymerize onto the nanoparticle surface for approximately 48hrs. This yielded silica coated nanoparticles with approximately 1-2 nm of silica as shown in the high resolution TEM image shown below in figure 10. Although not all silver nanoparticles were coated with silica, the presence of silica was confirmed on several nanoparticles by elemental analysis.

The effect of the silica coating on the SERS intensity was measured by comparing the Raman intensity from silver nanoparticles and silica coated nanoparticles in solution with 100

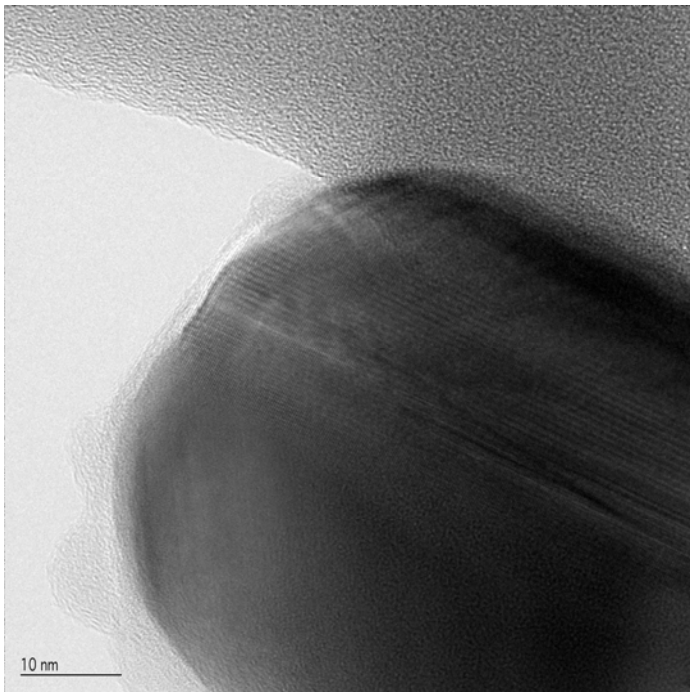

Figure 10 High resolution TEM image of a silver nanoparticle coated with silica. The rough silica coating can be seen on the outer edge of the silver nanoparticle and the presence of silica is confirmed with elemental analysis

nm Rhodamine 6G. The resulting spectra are shown in figure 11. As illustrated by the spectra, which were collected using 1.1 mW 633 nm, the intensity of the silica coated nanoparticles is approximately two orders of magnitude lower than the Raman intensity from the bare silver nanoparticles.

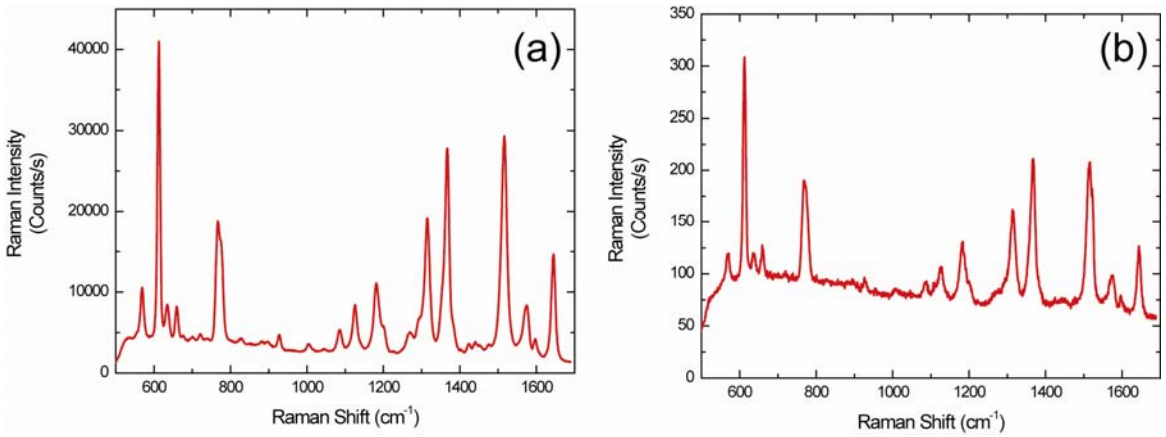

Figure 11 Bulk SERS measurements of R6G on uncoated (a) and silica coated (b) nanoparticles. The intensity of the Raman scattering is approximately two orders of magnitude lower for the silica coated nanoparticles.

While this is a good indication that the silica coating significantly reduces the scattering intensity, it is impossible to determine from the bulk measurements whether the reduction in signal intensity is the result of a small fraction of uncoated particles contriubuting a large signal when most of the coated nanoparticles produce no enhancement. In order to address this question, we performed SERS measurements and TEM measurements on the same coated nanoparticles. These results are shown in figure 12. The silica coated nanoparticles were incubated with 100 nm R6G and dried onto and indexed holey carbon coated TEM grid. Particles were located on the TEM grid in the confocal image shown in figure 12a and the selected nanoparticles were positioned over the focused laser while the SERS spectra were collected for 30 seconds. The TEM images of two nanoparticle clusters are shown in 12b and c with their corresponding SERS spectra shown below the respective TEM image in d and e.

The TEM images of the SERS active nanoparticle clusters show that the nanoparticles are coated with SiO_2. However, because of the large size and three dimensionality of the nanoparticle clusters, it is impossible to determine if all nanoparticle junctions are coated with SiO_2. More uniform SERS substrates which have recently been developed in our lab will need to be characterized using this technique in order to provide a more accurate measurement of the effect of having the molecule separated from the metal surface by an insulator.

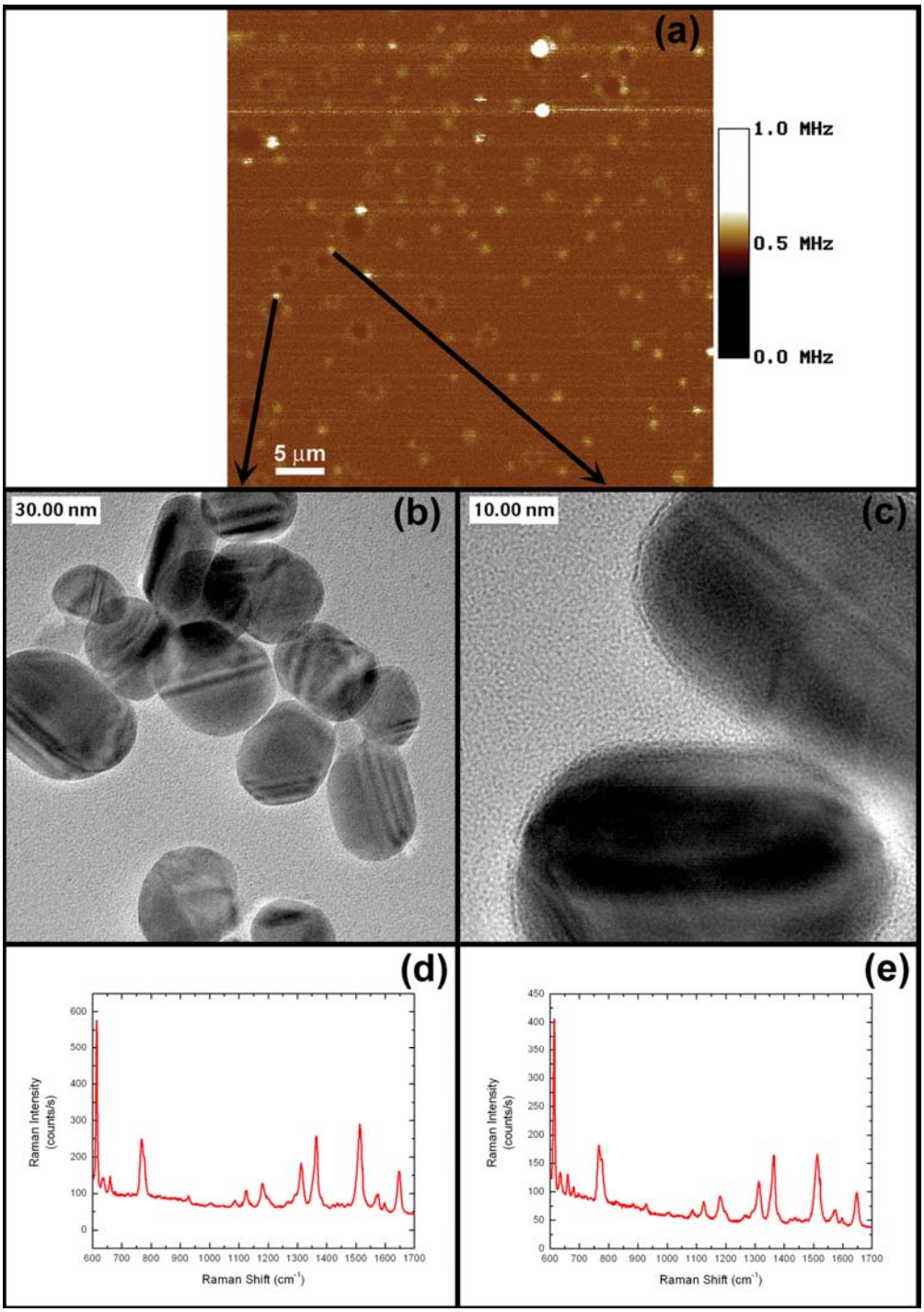

Figure 12 (a) Confocal image of silica coated nanoparticles on an indexed TEM grid. The nanoparticles are coated with silica. The HR-TEM images of two of the nanoparticle clusters are shown in (b) and (c). The respective SERS spectra of the R6G on the silica nanoparticles are shown below their respective TEM images in (d) and (e)

Exit Plan

We have begun discussons with Intel Corp. (Precision Biology Group) regarding the development of DNA sequencing technology based on SERS. In addition we are also planning to initiate discussions with Hewlett-Packard as another possible avenue for the fabrication of devices that could be used for SERS sequencing. Finally, once devices that have been designed through the modeling techniques developed in this project have been fabricated and tested, we will prepare and submit a grant application to NIH (NHGRI), which has recently announced a program for the development of novel sequencing technologies.

Summary

We have developed a numerical tool based on a quasi-static finite element approach for calculating the E-field and resulting SERS enhancements for metal nanostructure of arbitrary shapes and sizes. The results from calculations using this tool have shown that specially designed structures are capable of providing SERS enhancements which are approximately 12 orders of magnitude larger than for two adjacent spheres. These structures are designed such that they can be fabricated with currently available tools. Measurements of the additional enhancements attainable by combining SERS with CARS (SE-CARS), showed that an additional factor of two in the enhancement can be attained. This relatively small enhancement compared to the reported literature values is the result of local heating at higher power densities. Careful design of a SERS structure with the numerical tool developed may allow for additional enhancements using the SE-CARS approach. Finally, SERS measurements from silver nanoparticles coated with SiO_2 have shown that the loss of enhancement can be as large as 2 orders of magnitude with a small 1-2 nm coating of SiO_2 on the nanoparticle surface, compared to uncoated nanoparticles which have shown single molecule sensitivity.

Acknowledgements

This work was performed under the auspices of the U.S. Department of Energy (DOE) by the University of California, Lawrence Livermore National Laboratory (LLNL) under Contract No. W-7405-Eng-48. The project (05-ERD-080) was funded by the Laboratory Directed Research and Development Program at LLNL.

References

1. Service, R.F., SINGLE MOLECULES:Deconstructing DNA for Faster Sequencing. *Science*, (1999). **283**(5408): p. 1669-.
2. Meldrum, D.R., Sequencing Genomes and Beyond. *Science*, (2001). **292**(5516): p. 515-517.
3. Perkins, T.T., et al., Sequence-Dependent Pausing of Single Lambda Exonuclease Molecules. *Science*, (2003). **301**: p. 1914-1918.
4. Vercoutere, W., et al., Rapid Discrimination Among Individual DNA Hairpin Molecules at Single-Nucleotide Resolution Using an Ion Channel. *Nature Biotech.*, (2001). **19**: p. 248-252.
5. Werner, J.H., et al., Progress Towards Single-Molecule DNA Sequencing: A One Color Demonstration. *J. Biotech.*, (2003). **102**: p. 1-14.
6. Harris, T.D., J.J. Macklin, and J.K. Trautman. *Application of Ultra-Violet Single Molecule Detection to DNA Sequencing*. in *American Chemical Society National Meeting*. 1998. Dallas, TX.
7. Braslavsky, I., et al., Sequence Information can be Obtained from Single DNA Molecules. *Proc. Natl. Acad. Sci. USA*, (2003). **100**(7): p. 3960-3964.
8. Levene, M.J., et al., Zero-Mode Waveguides for Single-Molecule Analysis at High Concentrations. *Science*. **299**: p. 682-686.
9. Fleischmann, M., P.J. Hendra, and A.J. McQuillan, Raman Spectra of Pyridine Adsorbed at a Silver Electrode. *Chem. Phys. Lett.*, (1974). **26**(2): p. 163-166.
10. Jeanmaire, D.L. and R.P. Van Duyne, Surface Raman Spectroelectrochemistry Part I. Heterocyclic, Aromatic, and Aliphatic Amines Adsorbed on the Anodized Silver Electrode. *J. Electroanal. Chem.*, (1977). **84**: p. 1-20.
11. Albrecht, M.G. and J.A. Creighton, Anomalously Intense Raman Spectra of Pyridine at a Silver Electrode. *J. Am. Chem. Soc.*, (1977). **99**: p. 5215-5217.
12. Nie, S. and S.R. Emory, Probing Single Molecules and Single Nanoparticles by Surface-Enhanced Raman Scattering. *Science*, (1997). **275**: p. 1102-1106.
13. Kneipp, K., et al., Single Molecule Detection Using Surface-Enhanced Raman Scattering (SERS). *Phys. Rev. Lett.*, (1997). **78**(9): p. 1667-1670.
14. Xu, H., et al., Electromagnetic Contributions to Single-Molecule Sensitivity in Surface-Enhanced Raman Scattering. *Phys. Rev. E.*, (2000). **62**(3): p. 4318-4324.
15. Kneipp, K., et al., Ultrasensitive Chemical Analysis by Raman Spectroscopy. *Chem. Rev.*, (1999). **99**: p. 2957-2975.
16. Murray, C.A., D.L. Allara, and M. Rhinewine, Silver-Molecule Separation Dependence of Surface-Enhanced Raman Scattering. *Phys. Rev. Lett.*, (1980). **46**(1): p. 57-60.
17. Murray, C.A. and D.L. Allara, Measurement of the Molecule-Silver Separation Dependence of Surface Enhanced Raman Scattering in Multilayered Structures. *J. Chem. Phys.*, (1982). **76**(3): p. 1290-1303.
18. Ye, Q., J. Fang, and L. Sun, Surface-Enhanced Raman Scattering from Functionalized Self-Assembled Monolayers. 2. Distance Dependence of Enhanced Raman Scattering from an Azobenzene Terminal Group. *J. Phys. Chem. B*, (1997). **101**: p. 8221-8224.

19. Kennedy, B.J., et al., Determination of the Distance Dependence and Experimental Effects for Modified SERS Substrates Based on Self-Assembled Monolayers Formed Using Alkanethiols. *J. Phys. Chem. B*, (1999). **103**: p. 3640-3646.
20. Chew, H., D.-S. Wang, and M. Kerker, Surface Enhancement of Coherent Anti-Stokes Raman Scattering by Colloidal Spheres. *J. Opt. Soc. Am. B*, (1984). **1**(1): p. 56-66.
21. Prodan, E., et al., A hybridization model for the plasmon response of complex nanostructures. *Science*, (2003). **302**(5644): p. 419-422.
22. Nordlander, P. and E. Prodan, Plasmon hybridization in nanoparticles near metallic surfaces. *Nano Letters*, (2004). **4**(11): p. 2209-2213.
23. Talley, C.E., et al., Intracellular pH sensors based on surface-enhanced Raman scattering. *Analytical Chemistry*, (2004). **76**(23): p. 7064-7068.
24. Cheng, J.X. and X.S. Xie, Coherent anti-Stokes Raman scattering microscopy: Instrumentation, theory, and applications [Review]. *Journal of Physical Chemistry B*, (2004). **108**(3): p. 827-840.
25. Koo, T.W., S. Chan, and A.A. Berlin, Single-molecule detection of biomolecules by surface-enhanced coherent anti-Stokes Raman scattering. *Optics Letters*, (2005). **30**(9): p. 1024-1026.

[i] The scale is irrelevant as long as the size of the surface plasmon is much smaller than the wavelength of light.